06FFL-179

Experimental and Numerical Investigation of Split Injections at Low Load in an HDDI Diesel Engine Equipped with a Piezo Injector

Rickard Ehleskog, Valeri Golovitchev, Ingemar Denbratt and Sven Andersson
Chalmers University of Technology, Sweden

Carlo Alberto Rinaldini
University of Modena and Reggio Emilia, Italy

ABSTRACT

In order to investigate the effects of split injection on emission formation and engine performance, experiments was carried out using a heavy duty single cylinder Diesel engine. Split injections with varied dwell time and start of injection were investigated and compared with single injection cases. In order to isolate the effect of the parameters selected to investigate, other variables were kept constant. In this investigation no EGR was used. The engine was equipped with a common rail injection system with a piezoelectric injector. To interpret the observed phenomena, engine CFD simulations using the KIVA-3V code were also made.

The results show that a reduction in NO_x emissions and brake specific fuel consumption was achieved for short dwell times whereas they were increased when the dwell time was prolonged. No EGR was used so the soot levels were already very low in the cases of single injections. The results indicated, however, no increase in soot as a result of splitting the injection in two parts. Both HC and CO emissions were found to increase with split injections.

INTRODUCTION

The high fuel efficiency and high torque of the diesel engine has made it the obvious choice for heavy duty applications for a long time. However, the good characteristics of the modern super-charged high speed diesel engine makes it very suitable for car applications as well. This has led to a larger share of diesel cars among new personal car registrations in Europe. Additionally the road goods transport, *i.e.* diesel engines, has increased more than other means of transport the last decade [1]. Since all engines emit combustion products that can be harmful to the environment, this increment puts higher demands on the diesel engine from an environmental point of view as the transport sector stands for a big part of the total emissions. The authorities mean to minimize the future engine's negative effects on the environment is emission legislation.

Basically, there are two ways to handle the hazardous emissions and the future emission legislation; either by exhaust aftertreatment or by different strategies lower the in cylinder pollutant formation. In reality, a combination of these two ways will lead to the goal. One possible strategy to lower the pollutant formation is to use multiple injections which is an injection that is divided into two or more parts and can allow low emission combustion. One distinguishes between three basic types of multiple injections; pilot, post, and split injection. A pilot is a short injection that precedes the longer main injection, whereas a post is a short injection that comes after the main injection. Further, a split is simply an injection split into two or more parts of which neither is a pilot nor post. A multiple injection sequence can be composed of a combination of various injections. The focus of this project is on split injections and how the choice of strategy strategy can be used to reduce engine out emissions. The effects of injection timing as well as the dwell time between the two parts of the split injection are investigated.

Split injection is a strategy where the injection is divided into two (or more) pulses. A second injection shortly after the first widens the region of high turbulent kinetic energy which enhances the evaporation and mixing processes and leads to better air utilisation and faster combustion. Consequently, split injections have an impact on the combustion and can be used to control combustion noise and emission formation. It have been found in earlier studies that a split injection increases the soot oxidation process in the late stages of the combustion process. This allows the injection to be retarded to reduce NO_x emissions while keeping soot levels konstant [2, 3, 4, 5]. More fundamental investigations on split injections like spray studies where the effect of split injections on spray formation and fuel/air mixture is investigated, are also found in the literature, *e.g.* [6, 7]. It has been shown that splitting the injection in two (or more) parts has a significant effect on the fuel/air mixing process and also that parameters such as dwell time and fuel mass distribution between the two injections are important in order to get the desired spray characteristics. In an experimental spray study Amagi *et al.* [8] showed that the ignition delay was shortened with a split injection and that it promoted a stabilisation of the combustion as a result of the enhanced mixing process. Obviously, there are several parameters of the split injection that have an influence on the combustion process. Dwell time and the duration of each pulse are already mentioned but other parameters such as injection rate, start of injection etc. are important as well. These parameters are important and must be optimized in order to maximize the effect of the split injection. The parameters in focus in this study are start of injection and dwell time. For a too short dwell time the second injection will replenish the already fuel rich region of the first injection pulse with more fuel leading to further soot formation, while for a too long dwell time the second pulse will be injected in to a lower temperature region leading to an increased combustion duration.

EXPERIMENTAL SETUP

In order to investigate, and find an explanation to the effect of splitting a single injection in two parts a series of tests were was performed. Split injections with four different dwell times, 1.4-4.4 CAD, were investigated and compared with single injections as reference cases. These five cases will be referred to as case 1 to case 5 or reference case, $split_{1.4}$, $split_{2.4}$, $split_{3.4}$ and $split_{4.4}$. The five injection sequences were investigated at four starts of injection (SOI); -10, -5, 0 and 5 CAD aTDC. Since a separation of two injection pulses with constant SOI results in a retarded combustion, the centre of the injection control signal was kept constant when the injection was split in two parts and when the dwell time was increased. This means that the start of injection, and thus the start of combustion, is advanced when the injection is separated, see Figure 1. Therefore, *e.g.* a split injection with a dwell of 2.4 CAD will have a SOI that is advanced 1.2 CAD ($^1/_2$ dwell time) compared to the single injection. This generates the test matrix of 20 points in total, see Table 1. Although all cases have different SOI they are referred to as groups with SOI at -10, -5, 0 and 5 CAD aTDC.

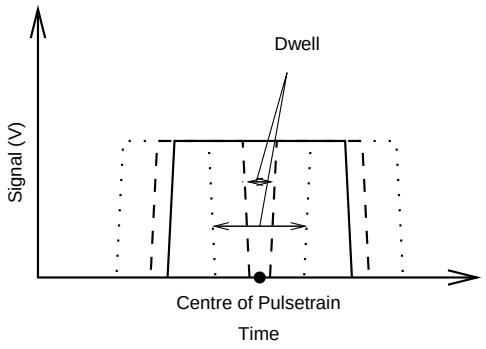

Figure 1: The injections are separated while the centre of the injection sequence is kept at a constant timing. The figure shows the pulse trains for a single injection and two split injections with different dwell times

Table 1: Test matrix

Inj. sequence	SOI aTDC (CAD)	Dwell time (CAD)	Appelation
Single	**-10**	–	ref. case, SOI -10
Split	-10.7	1.4	$split_{1.4}$, SOI -10
	-11.2	2.4	$split_{2.4}$, SOI -10
	-11.7	3.4	$split_{3.4}$, SOI -10
	-12.2	4.4	$split_{4.4}$, SOI -10
Single	**-5**	–	ref. case, SOI -5
Split	-5.7	1.4	$split_{1.4}$, SOI -5
	-6.2	2.4	$split_{2.4}$, SOI -5
	-6.7	3.4	$split_{3.4}$, SOI -5
	-7.2	4.4	$split_{4.4}$, SOI -5
Single	**0**	–	ref. case, SOI 0
Split	-0.7	1.4	$split_{1.4}$, SOI 0
	-1.2	2.4	$split_{2.4}$, SOI 0
	-1.7	3.4	$split_{3.4}$, SOI 0
	-2.2	4.4	$split_{4.4}$, SOI 0
Single	**5**	–	ref. case, SOI 5
Split	4.3	1.4	$split_{1.4}$, SOI 5
	3.8	2.4	$split_{2.4}$, SOI 5
	3.3	3.4	$split_{3.4}$, SOI 5
	2.8	4.4	$split_{4.4}$, SOI 5

Since the injection timings, SOI and dwell time, discussed above refer to the control signal rather than the actual injection, the injection sequences them

selves look somewhat different. There are two major factors that affect how the real injection differs from the control signal, or pulse train, sent to the injector. First, it takes some time to open and close the injector. Second, if there is more than one injection, as for a split injection, the first injection will cause the pressure in the fuel system to fluctuate, and because the opening and closing of the injector as well as the injection rate is dependent of the fuel pressure, the timing and shape of the second injection will depend on the preceding injection and the dwell time between the two injections. Since the piezo injector could not be equipped with a needle lift sensor, there is no easy way to observe the injector operation during the engine tests. Instead the used injection sequences has been measured in an atmospheric spray chamber using an impingement method [9, 10]. The measured profiles for SOI -5 CAD aTDC are plotted in Figure 2. It can be seen that the centre of the injection sequences are kept almost at the same position for all cases. On the other hand, the injection sequences are not shaped perfectly as 50-50 % split injections. The two injection parts differ both in duration and rate. In the $split_{1.4}$ case there are not even two separated injections. Instead, there is only a short drop in rate. The reason is that the two parts are too close to each other for the injector to fully close. For the other three split sequences, two separate injections are distinguished even though they differ somewhat in rate and duration. As mentioned before, the reason for this is the pressure fluctuations in the injection system caused by the opening and closing of the injector during the first injection. This has an as impact on both the opening and closing of the injector and the injection rate.

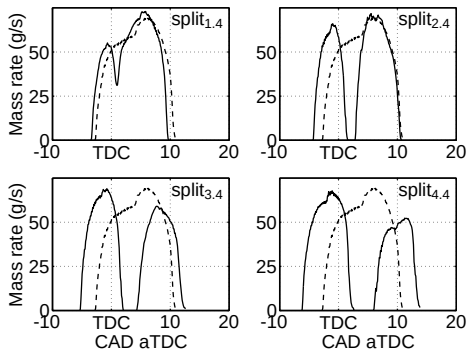

Figure 2: Real injection profiles for SOI -5 CAD aTDC. The set dwell times are indicated in the upper right corner of each plot. The reference case is represented by the dotted line

The experimental part of the project was performed in a single cylinder research engine from AVL. It has a cylinder head with a geometry based on a Volvo D12C

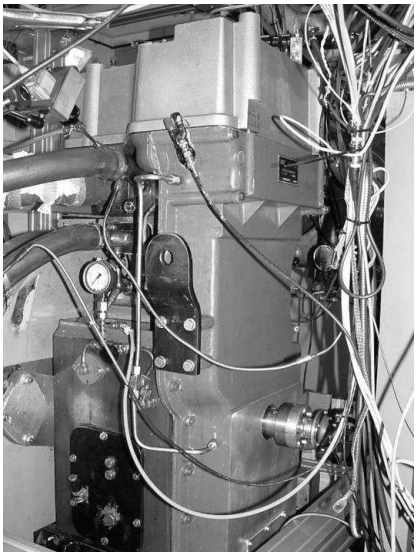

Figure 3: The AVL single cylinder research engine

Table 2: Engine and fuel injection system specification

Engine	Single cylinder, AVL 501
Cylinder head	Volvo D12C 3 (4) valves
Bore	131 mm
Stroke	150 mm
Displacement	2.022 l
Compression ratio	18.5
Fuel injection system	Common rail (max. pressure 1800 bar)
Injector	Piezo-electric
Nozzle	7 .147 mm orifices, 140° umbrella angle, 440 g/30s flow rate

engine with a displacement of 2 litre. During this investigation it was equipped with a common rail injection system with a piezo-electric injector. The specification of the engine and fuel injection system is listed in Table 3.

The experiments were performed at 1200 rpm and constant load at 75 Nm (25 %). No exhaust gas recirculation was used during the investigation. In order to isolate the effect of the investigated parameters other variables were kept constant if possible.

Table 3: Engine operating conditions

Speed	1200 rpm
Load	25 % (75 Nm)
SOI	-10, -5, 0 & 5 CAD aTDC
Charge air pressure	115 mbar
Injection pressure	1500 bar

COMPUTER MODELING

The numerical simulations were carried out for one set (SOI -5 CAD aTDC). The techniques used in the modelling are briefly described below.

DIESEL FUEL SURROGATE CHEMISTRY MODEL Practical diesel fuels consist of a great number of aliphatic and aromatic compounds, and their combustion is too complex to be modelled using a comprehensive chemical mechanism. Instead of this, model or surrogate fuels are used in numerical simulations. Aliphatic components can be represented by long chain hydrocarbons such as *n-heptane* or *n-dodecane* due to their cetane number of approximately 56, which is similar to the cetane number of conventional diesel fuels. Aromatic components significantly contribute to soot formation. The diesel fuel surrogate, which can sufficiently represent the cetane number as well as the other properties of real fuel, is assumed to be a 70/30 $\%$ blend of n-heptane, C_7H_{16}, and toluene, C_7H_8.

At first detailed reaction mechanism for *n-heptane* and toluene oxidation has been developed (72 species, 306 reactions) and validated using shock-tube auto-ignition experimental data. The results of such a comparison is presented in Figure 4 illustrating reasonable agreement between predictions and measured ignition delays.

It is instructive to note that NTC (Negative Temperature Coefficient) features in the ignition delay time vs. time history is well pronounced for *n-heptane* but barely visible for toluene. The NTC feature is also poorly pronounced for diesel oil surrogate. The ignition delay times for the surrogate at low temperatures were predicted shorter for *n-heptane* due to usage of the global oxidative pyrolysis stage in a form:

$$1.5C_{14}H_{28} + 0.5O_2 \rightarrow 2C_7H_{16} + C_7H_8 + H_2O \quad (1)$$

This ignition peculiarity is in compliance with real diesel oil spray auto-ignition in a constant volume.

To predict soot formation, the kinetics of aromatics till gaseous soot precursors supposed to be acenaphthylene A2R5, was integrated into the combustion chemistry. To accurately predict NO formation described by the extended Zel'dovich mechanism,

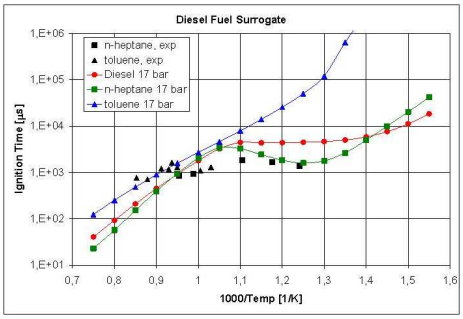

(a) p_0 = 17 bar, Φ=1

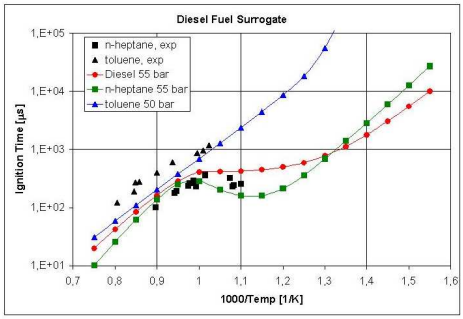

(b) p_0 = 55 bar, Φ=1

Figure 4: Ignition delays for fuel surrogate and its components from simulating shock-tube experiments

$$O + N_2 \rightleftarrows NO + N \quad (2)$$
$$N + O_2 \rightleftarrows NO + O \quad (3)$$
$$OH + N \rightleftarrows NO + H \quad (4)$$

it is necessary to remove the trace species (species in low concentration) from the left-hand side of this reaction. If this is not done, artificially small effective reaction rates may result. The problem is that, unless the time step is unacceptably small, the progress of such a reaction may be prematurely halted by the depletion of trace species on a single time integration step. The remedy suggested in the KIVA code was replaced by another equivalent approach: the partial density values of trace species could not be less than 1.e-9. With this assumption, a reasonable agreement between predictions and experimental data has been achieved. The presence of other species as N_2O and NO in the reaction mechanism introduced no problem in the numerical treatment.

TURBULENCE-CHEMISTRY INTERACTION MODEL The new model formulation is based on a time-splitting procedure applied to the mass conservation equation. In accordance with this approach the time differencing was performed in

three steps: the first step was assumed to be the convection contribution, the second one was concerning the diffusion effect without a contribution of micro-mixing, and the third step was the chemical kinetics effect coupled with micro-mixing. The last step of such a mass balance can be interpreted as representing combustion in a constant volume partially stirred reactor (PaSR) of a computational cell size, where reactions occur in a fraction of its volume. Since the reaction zone parameters as a rule can not be resolved on a computation grid, the sub-grid diffusion term due to micro-mixing was approximated with the help of introduction of a micro-mixing time as suggested in the "interaction with the mean" approach. The micro-mixing is connected with a cascade mechanism between large and small scales. Then, assuming that the chemical process proceeds in such a way that the shortest chemical time associated with particular (reference) species participating in the reaction was constrained by the micro-mixing time, a system of PaSR equations consisting of two sets can be obtained from the rate diagram presented in Figure 5

$$\frac{dc_1}{dt} = \frac{c_1 - c_0}{\tau} = \frac{c}{\tau_c}, \quad -\frac{c}{\tau_c} = \frac{c - c_1}{\gamma(c_1)\tau_{mix}} \tag{5}$$

where τ is the time step, τ_c is the chemical reaction time, τ_{mix} is the micro-mixing time and γ_{c_1} is a mixing progress variable. The model distinguishes between the concentration (in mean molar density) at the reactor exit, c_1, the concentration in the reaction zone, c, and in the feed c_0. When time proceeds, c_0 trades places with c_1. Unlike the previous model formulation [11], a new multiplier $\gamma(c_1)$ is introduced aiming "to place" the point C on a straight line in the Figure 5 to assure the formal implementation of the 2nd equation in Eq. 5.

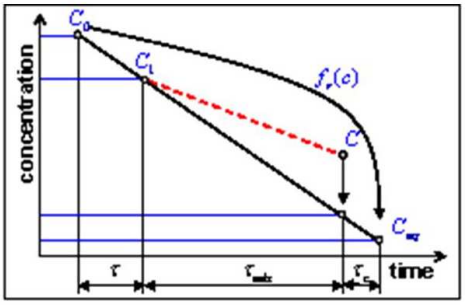

Figure 5: Schematic rate diagram of PaSR model

The definition of the mixing progress variable depends on the combustion regime. For the case of conventional diesel combustion, this coefficient is taken as described in Kong *et al.* [12], *i.e.*

$$\gamma = \frac{1 - e^{-r}}{0.632}, \quad r = \frac{\sum_{i=i_{prod}} Y_i}{1 - Y_{air}} \tag{6}$$

where r denotes the product mass fraction in the mixture composition. After algebraic manipulations, one can yield the analytical solutions of the above problem which finally can be represented as

$$\frac{c_1 - c_0}{\tau} = -\left(\frac{c_1}{\tau_c}\right)\kappa = \frac{1}{2}H\left(\frac{c_1}{\tau_c}, \frac{c_1}{\gamma(c_1)\tau_{mix}}\right) \tag{7}$$

where $\kappa = \tau_c/(\gamma(c_1)\tau_{mix} + \tau_c)$ and *H* is a harmonic mean. For the detailed chemical mechanism, the species production rate to the particular r-chemical reaction (separated into creation and destruction rates) contrary to the 1st equation of the system can be written as

$$\frac{dc_1}{dt} = f_r(c) = \frac{c - c_1}{\gamma(c_1)\tau_{mix}} \tag{8}$$

where

$$f_r(c) = (\upsilon_r'' - \upsilon_r')\dot{\omega}_r(c) = term_r^+ - term_r^- \tag{9}$$

and υ_r'' and υ_r' are stoichiometric coefficients of the backward and forward stages and $\dot{\omega}_r$ is a progress variable rate of the rth-reaction. Species indices are omitted for simplification. The reaction progress variable rate $\dot{\omega}_r(c)$ is calculated from the mass-action law

$$\dot{\omega}_r(c) = k_f^r(T)\prod_{S=1}^{N_s}(c_s)^{\upsilon_{Sr}'} - k_b^r(T)\prod_{S=1}^{N_s}(c_s)^{\upsilon_{Sr}''} \tag{10}$$

where k_f^r and k_b^r are the rate coefficients for the forward and backward stages of the r-reaction in the mechanism, *T* is the temperature and N_s is the number of species in the mixture. In this case, the reaction rate Eq. 7 takes the form

$$\frac{c_1 - c_0}{\tau} = f_r(c_1)\kappa = \frac{c_0 f_r^0}{c_0 + term_r^-\tau - term_r^-\gamma(c_1)\tau_{mix}} \tag{11}$$

containing no reaction zone parameters *c* which cannot be resolved on a grid, but replacing their effect with the rate multiplier κ. The definitions of micro-mixing and reaction times are described in Golovitchev *et al.* [11].

ABOUT THE NUMERICAL RESULTS The computer modelling part of this paper include simulations of the five cases with SOI at -5 CAD aTDC, *i.e.* one reference case and four cases with split injections, case 1 to case 5. The computational model developed has been applied to simulation of the axisymmetric bowl-in-piston with a peak in the center of the bowl. In the simulations, the 360-degree polar mesh ($57\times100\times36$ cells in the squish region + $32\times100\times20$ cells in the bowl region), see Figure 6, and 51.4285 degree sector mesh ($57\times20\times36$ cells in the squish region + $32\times20\times20$ cells in the bowl region) have been employed. On the sector mesh, only one spray was accounted for, while all seven sprays were accounted for on the polar mesh. For each experimental case the injection velocity profiles, injection durations and individual spray and droplet parameters were specified. In particular, the injection profiles and injected mass vs. crank angle histories are presented in Figure 7 and 8. Since simulation on the polar mesh is time-consuming, the calculations for cases 2 and 5 were repeated on the sector mesh and integrated in-cylinder parameters, such as pressure and rates of heat release (RoHR) were compared with those calculated on the polar mesh. The results of this comparison are presented in Figure 9 and 10. Since the results obtained on both meshes are found to be consistent, a major part of the simulations of the experimental cases listed in Table 4 is performed on the sector mesh.

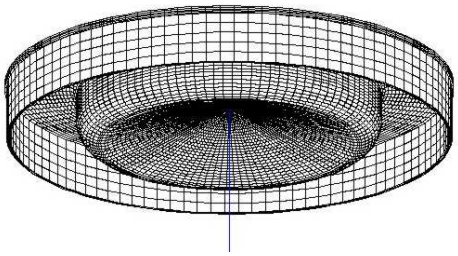

Figure 6: Computational polar mesh for the Volvo D12C engine

The results of a comparison of the calculated volume averaged in-cylinder pressure for case 2 with experimental data are presented in Figure 11. Some deviations from the experimental results are evident, but the general trend is similar and the deviations can be explained. The in-cylinder pressures appeared

Table 4: The injection parameters for the case under study

	Case 1	Case 2	Case 3	Case 4	Case 5
n	136	133	152	181	202
SOI	-2.766	-3.468	-4.366	-5.366	-6.266
InjD	9.86	9.5	10.9	13	14.5
Mass	70.05	67.99	67.72	70.16	72.53
Δ CAD	.07197	.07197	.07219	.07222	.07214

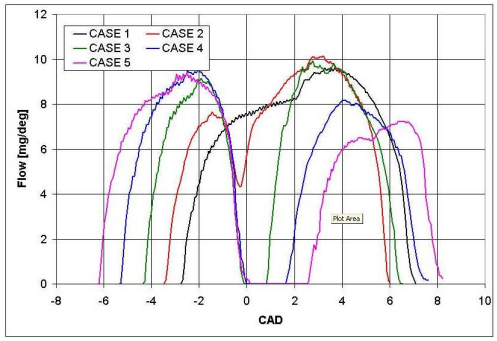

Figure 7: Injection profiles vs. crank angle history for the cases studied

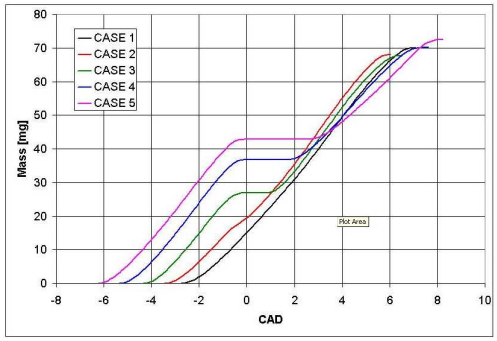

Figure 8: Mass injected vs. crank angle history for the cases studied

to be under-predicted for both cases, while the peak pressures are over-predicted. Also RoHR and integrated heat release were compared. The ignition phasing (start of ignition and peak RoHR) and general shape of RoHR were predicted correctly. However, the RoHR values were over-predicted, resulting in higher in-cylinder pressures. The value of RoHR has been calculated using a direct summation of thermal effect of chemical reactions in a cylinder volume. When the RoHR profiles are integrated to give accumulated heat release values, the predicted values are very close to the theoretical heating value (44.8 MJ/kg) which is higher than the experimental value. Regardless of these deviations, the simulations were used to interpret experimental results.

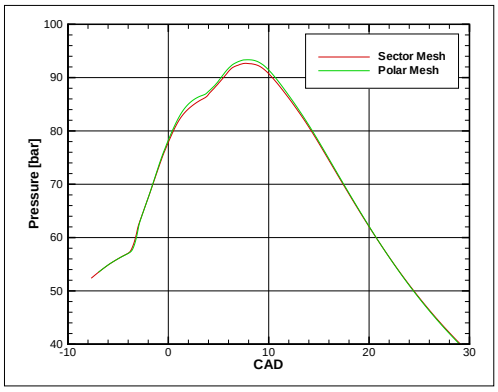

Figure 9: Predicted pressure vs. CAD histories for Case 5 obtained on the polar and sector meshes

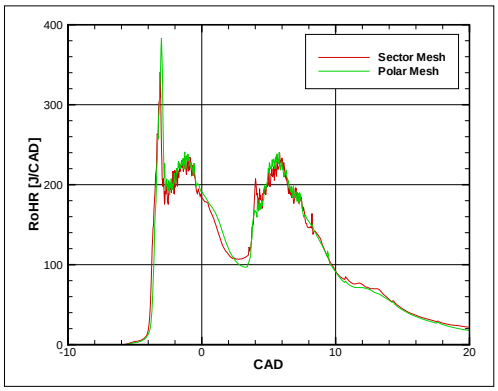

Figure 10: Predicted Rate of Heat Release vs. CAD histories for Case 5 obtained on the polar and sector meshes

RESULTS AND DISCUSSION

Typical simulation results on the polar mesh can be seen in a gallery of reacting mixture parameters (temperature, oxygen, CO and NO mass fractions) for different crank angles for case 2 and 5 in Figures 13 to 16. These distributions are referred to a plane which is normal to the cylinder axis crossed just below the engine squish plane. Case 2 and 5 represent the cases with the most differing time dwells between injection pulses (1.4 and 4.4 CAD respectively). The spatial distribution of temperature (in deg K), oxygen, NO and CO in mass fraction are presented in Figures 13, 14, 15 and 16, respectively.

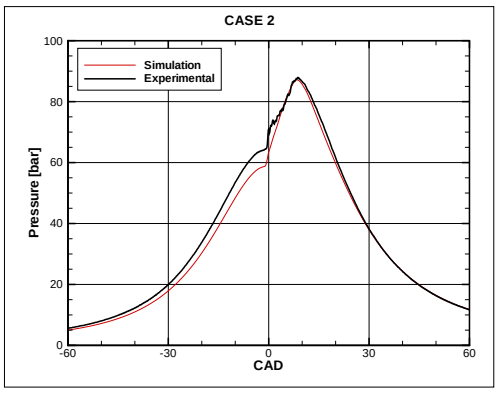

Figure 11: Comparison with experimental pressure of volume averaged data vs. CAD histories for case 2 obtained on the sector mesh.

In Figure 12(a), the engine out NO_x emissions are plotted as a function of the dwell time between the split injections. According to the curves, a split injection with a short dwell has a reducing effect on the NO_x emissions whereas a longer dwell increases the NO_x emissions to a higher level compared to the reference cases. It is also clear that a late injection gives lower NO_x. This can be seen clearly when the NO_x emissions are plotted against the start of combustion, Figure 12(b). The later the ignition occurs, the lower the NO_x emissions. However, a split with a short dwell time seems to lower the NO_x production.

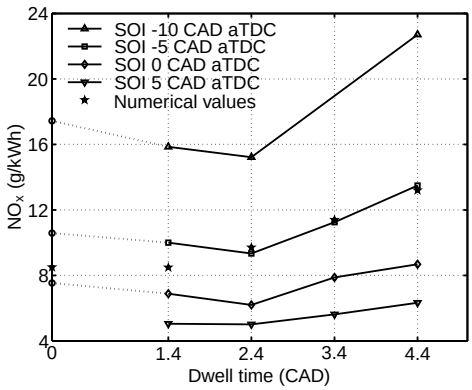

(a) NO_x vs. dwell time, including numerical values for SOI -5 CAD aTDC

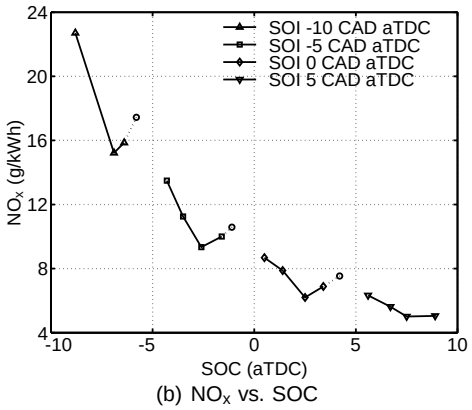

(b) NO_x vs. SOC

Figure 12: Engine out emissions of NO_x. Circles connected with dotted lines mark the reference cases

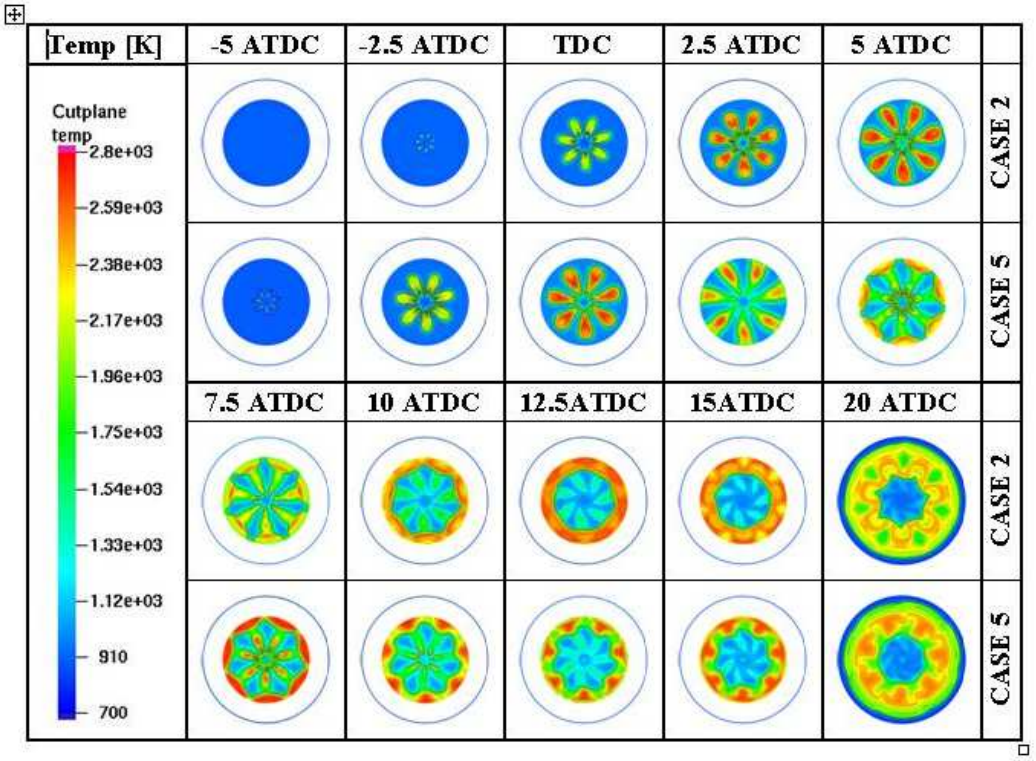

Figure 13: In-cylinder temperature distribution calculated on the polar mesh for cases 2 and 5

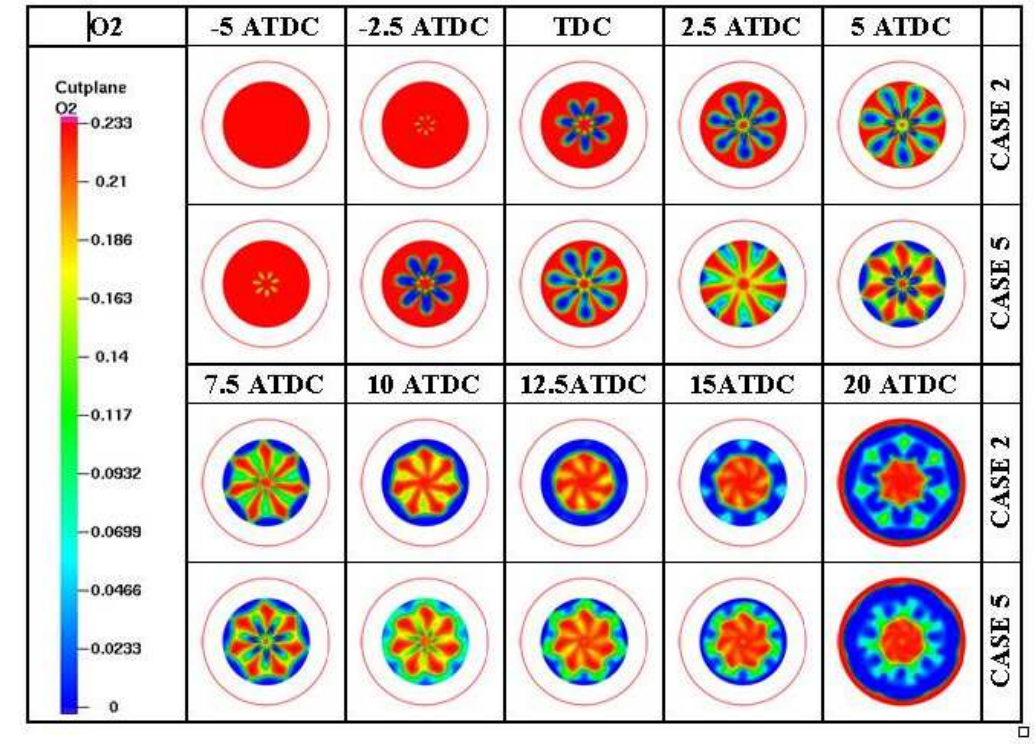

Figure 14: In-cylinder O_2 distribution calculated on the polar mesh for cases 2 and 5

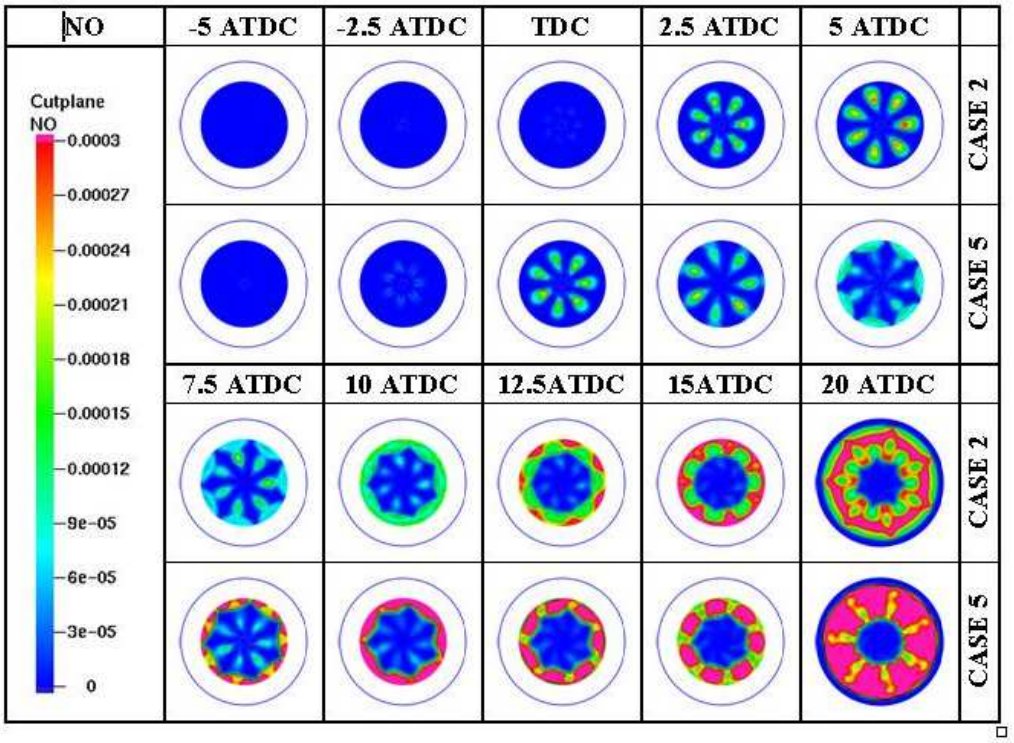

Figure 15: In-cylinder NO distribution calculated on the polar mesh for cases 2 and 5

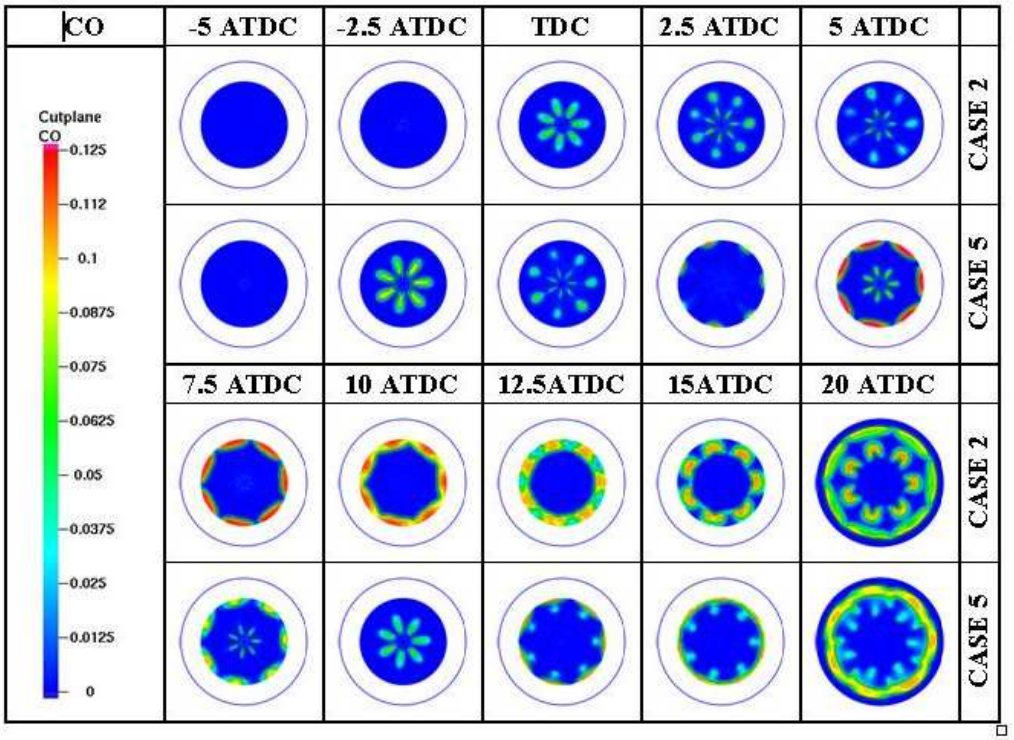

Figure 16: In-cylinder CO distribution calculated on the polar mesh for cases 2 and 5

From simulated temperature distributions, see Figure 13, it follows that in the case of early injection (case 5) combustion starts early and develops more rapidly for the first injection pulse. The combustion starts in the vicinity of each spray forming well pronounced plumes. The evidence of the second pulse is very clear for case 5 at 5 CAD aTDC. The same thing can also be seen in the O_2 distribution (see Figure 14) where regions with reduced amount of oxygen appeare. The oxygen distributions for case 5 at -2.5 and 5 CAD aTDC show that the oxygen consumed in the first pulse affects NO production as can be seen in Figure 15. Figure 15 also show how the NO formation in the plume zone stops for case 5 at 5 CAD aTDC, but resumes again at 7.5 CAD aTDC, since the "oxygen holes" are replenished during the dwell between injections. In the case of considerably separated injections this can result in higher NO emissions as was observed in the experiments. Therefore it is important to optimize injection parameters such as dwell time when multiple injections are being used to reduce NO_x emissions

The integrated NO values from the simulations of cases 1-5 are presented in Figure 17. As mentioned above, the amount of engine out NO was overpredicted for case 5 with the longest dwell time. The predicted integrated amount of NO compared to experimental values for case 1 to 5 presented in Figure 12(a) show reasonable agreement.

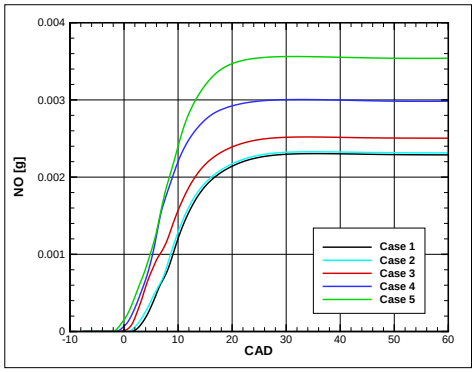

Figure 17: In-cylinder NO vs. CAD histories for cases 1-5 calculated on the sector mesh

The soot emissions, see Figure 18, are close to the minimum level of the measuring instrument and therefore a analysis of the soot emission results is difficult to perform. The experimental results did not, however, indicate any increase in soot as a result of splitting the injection in two parts. The simulations also predicted low engine out soot emissions. The integrated soot values for cases 1-5 are presented in Figure 19. In the course of combustion process development two soot peaks are evident corresponding to two injections. The first peak value is highest for the case with the longest dwell. As a rule, a higher first maximum leads to a reduced second one.

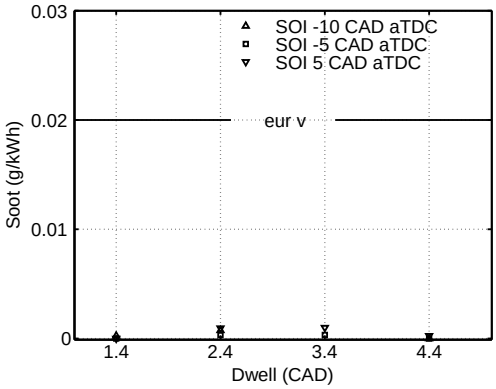

Figure 18: Engine out emissions of Soot compared to the Euro V limit

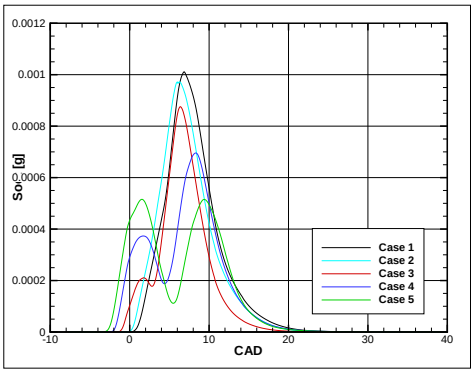

Figure 19: In-cylinder soot vs. CAD histories for cases 1-5 calculated on the sector mesh

The engine out CO emissions are increased by splitting the injection into two parts, Figure 20(a). However, the CO levels seem to decrease with increased dwell time. If the CO emissions are plotted against start of combustion, Figure 20(b), it can be seen that the earlier start of combustion, the lower the CO emissions are. This can in part be explained by the ignition delay which tends to decrease with later SOI (SOI 5 CAD aTDC excluded). Three possible reasons for high CO levels are; over-lean mixture; insufficient mixing rate (locally fuel rich); and low temperature. At fuel rich conditions the CO emissions increase with increasing fuel/air equivalence ratio. Since diesel engines operate at lean conditions, this is generally not a problem. However, if the fuel/air mixing process is insufficient, combustion in fuel rich areas will occur. The low O_2 levels will then preclude the formation of OH-radicals which is needed for the CO oxidation according to

$$CO + OH \rightarrow CO_2 + H \qquad (12)$$

Since the reaction in equation 12 has a low activation energy, it is not the CO oxidation process itself that is affected negative by a low temperature. Instead it is lack of OH-radicals that reduces the rate at which CO is converted to CO_2 at low temperatures [13]. A over-lean mixture is approaching the flammability limits causing incomplete combustion.

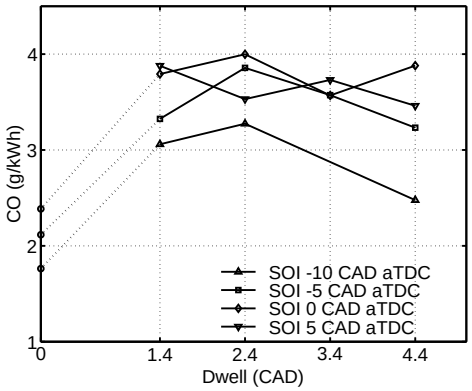

(a) CO vs. dwell time

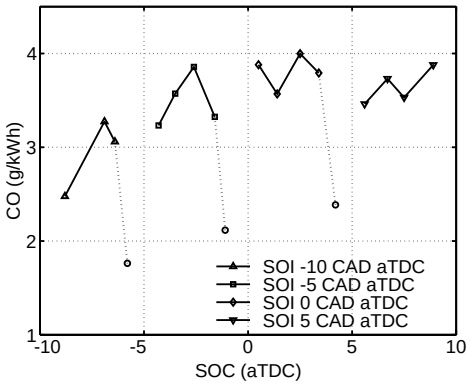

(b) CO vs. SOC

Figure 20: Engine out emissions of CO. Circles connected with dotted lines mark the reference cases

The areas where CO is produced according to the simulations are illustrated in Figure 16. If this gallery is compared with the temperature and O_2 galleries, Figures 13 and 14, two facts can be stated. First, in the CO richer areas the temperatures are relatively high. Therefore, a too low production of OH-radicals is not likely to be the cause of high CO levels. Second, the areas with high CO levels are the areas where the lowest O_2 levels occur. Hence, under-mixing and locally fuel-rich areas are a probable explanation of the high CO levels.

The numerical results represent the trends in the experiments only partially for the integrated CO emissions. However, when comparing the four experimental cases in Figure 20(a) it is found that there are no clear trends here neither. This is one reason why a correct numerical prediction could be difficult to perform.

Splitting the injection in two parts increases the engine out HC emissions, Figure 21. However, from these results it is difficult to say how the dwell time influences the HC level, and no clear effect of the start of combustion is detected.

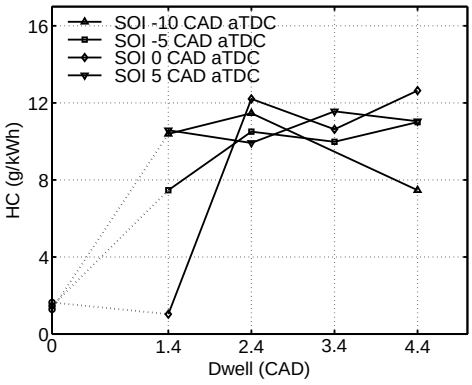

(a) HC vs. dwell time

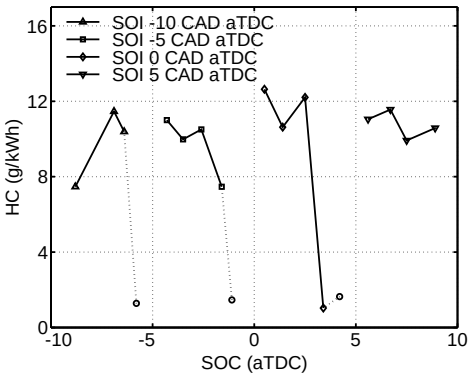

(b) HC vs. SOC

Figure 21: Engine out emissions of HC. Circles connected with dotted lines mark the reference cases

Since the diesel combustion process is very complex, there are many mechanisms that can affect the engine out HC emissions. The HC formation mechanisms can be divided in two groups; for fuel injected before ignition; and for fuel injected after ignition, *i.e.* during combustion. For the first group it is believed that over-lean mixture is the most important cause of high HC emissions. For the latter group it is mainly low mixing of fuel and air causing over-rich mixture or quenching that is causing incomplete combustion and emission of HC. Especially the fuel injected at a slow velocity in the late part of the injection is likely to be a source of HC [14]. Engines running at low load, as is the case for this study, are also producing higher amounts of HC. However, as in the case of CO emission it is probable that it is under-mixing and locally fuel rich areas that is the major cause for the HC emissions.

Rate of heat release (RoHR) for SOI -5 CAD aTDC are plotted in Figure 22, both versus CAD (plots on

the left hand side) and versus CAD after start of combustion (plots on the right hand side). The trends are the same for the other three injection timings, and therefore only this case is presented. Since the start of injection is earlier for the split injections compared to the reference case and also earlier with increased dwell time, the start of combustion and hence the rate of heat release is advanced for these cases. This can be seen by looking at the position of the peak of premixed combustion in the plots on the left hand side. Unlike for the premixed combustion, the time at which the mixed-controlled combustion takes place is more or less the same for all injection sequences. This indicates that the gradient of the rate of heat release after the premixed combustion must be higher for the reference case and the split cases with short dwell compared to the split cases with longer dwell. This can also be seen in the plots on the right hand side. Looking at the end of the combustion, there are differences between the cases, sequences that start late also end late but the difference is smaller at the end than at the start of combustion. Hence, a split injection with long dwell has a longer duration compared to shorter dwells and single injections, see Figure 23. However, the case with the latest injection, SOI at 5 CAD aTDC, follows the opposite trend. A possible reason for this is that the combustion takes place at a lower temperature as a result of the late injection, see the cylinder pressure in Figure 24. Split injections with short dwell and single injections also result in a higher maximum rate of heat release during the mixing controlled part of the combustion. All together this means that long dwell times give long combustion durations and low rate of heat releases but with slightly advanced start of combustion compared to shorter dwells and single injections.

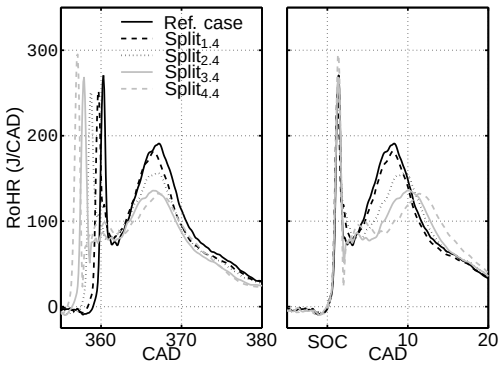

Figure 22: Rate of heat release, SOI_{-5}.In the diagram on the right hand side the RoHR is plotted versus CAD after start of combustion

The experiments show that a split injection with short dwell time decreases the brake specific fuel consumption (BSFC) compared to the reference case, Figure 25. The earlier SOI of the $split_{1.4}$ case results in a combustion that take place closer to TDC, see Figure 22. In this figure it can also be seen that the $split_{1.4}$ case has the shortest duration as well. Together, this makes the $split_{1.4}$ case the best regarding fuel economy. When the dwell time is increased, the fuel consumption increases and it finally becomes higher than for the reference case. The fuel consumption is also presented in mg/stroke in Table 5.

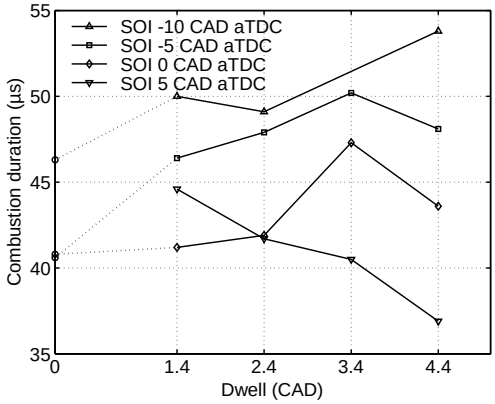

Figure 23: Combustion duration. Circles connected with dotted lines mark the reference cases

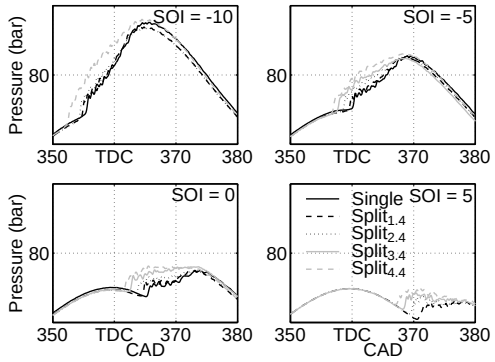

Figure 24: Cylinder pressure

The combustion efficiency can be calculated from the specific emissions of CO and HC and the brake specific fuel consumption according to

$$\eta_c = \frac{1 - \left(HC_{sp} + CO_{sp} \frac{LHV_{CO}}{LHV_{fuel}} \right)}{BSFC} \qquad (13)$$

where LHV is the lower heat value for CO and the fuel respectively. It is assumed that the heating value for HC is the same as for the fuel. The result from this calculation is presented in Table 6. Nearly compleat combustion is achieved for all reference cases presented, and is lower for all but one of the split

injection cases. The lower combustion efficiency together with the prolonged combustion duration, see Figure 22, is probably the reason for the increment in fuel consumption with increased dwell time.

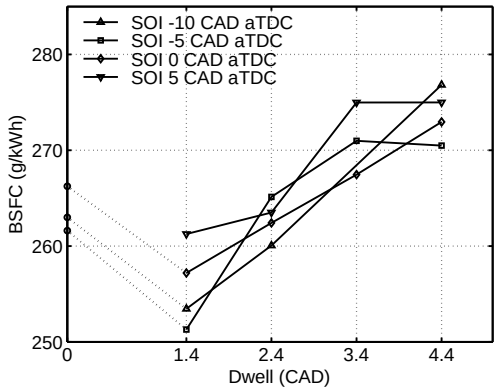

Figure 25: Fuel consumption vs. dwell time. Circles connected with dotted lines mark the reference cases

Table 5: Fuel per stroke (mg)

Dwell SOI	–	1.4	2.4	3.4	4.4
-10	70.1	68.4	67.9	–	72.3
-5	70.0	68.1	67.7	70.4	72.5
0	70.3	67.0	69.5	73.2	70.1
5	–	70.1	73.4	71.5	72.1

Table 6: Combustion efficiency

Dwell SOI	–	1.4	2.4	3.4	4.4
-10	.99	.96	.95	–	.97
-5	.99	.97	.96	.96	.96
0	.99	.99	.95	.96	.95
5	–	.96	.96	.95	.96

The in-cylinder parameters (pressure, RoHR, temperature, integrated heat turbulent kinetic energy and turbulent viscosity) calculated on the sector mesh for cases 1-5 are presented in Figures 26-31. From in-cylinder vs. CAD histories (see Figure 26) it follows that an increase of the dwell time resulting in advanced injections leads to an earlier start of combustion and a higher peak pressure. This is in compliance with the experimental data. From RoHR distributions presented in Figure 27 it follows that an advanced injection is associated with reduced initial peak value. Later on, the presence of the second injection pulse causes first one and then a second maxima on the RoHR curve. This is also in agreement with experimental results.

From volume averaged temperature vs. CAD distributions (see Figure 28) it follows that in the case of advanced injection, an increased longest dwell time

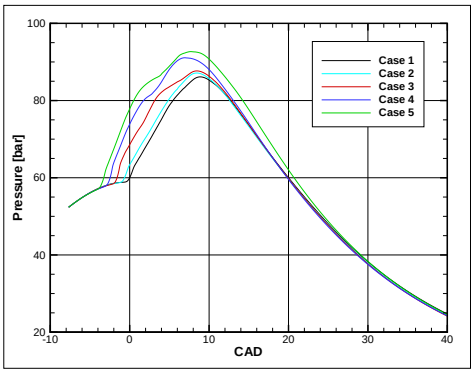

Figure 26: In-cylinder Pressure vs. CAD histories for cases 1-5 calculated on the sector mesh

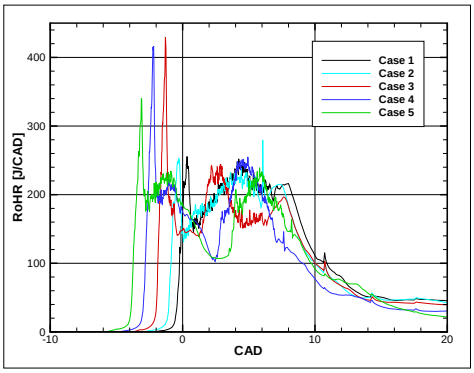

Figure 27: In-cylinder RoHR vs. CAD histories for cases 1-5 calculated on the sector mesh

results in a delayed maximum value of the temperature. The maximum value corresponds to the case with the longest dwell. Integrated heat release were predicted to be nearly identical with the experimental data, testifying to the complete combustion (see Figure 29).

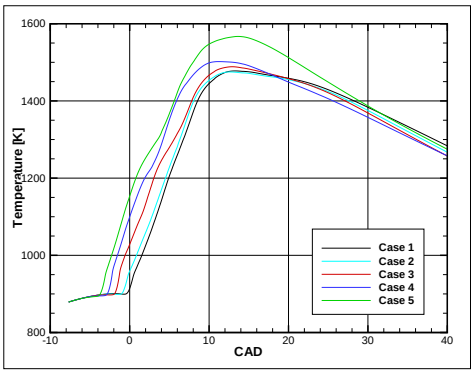

Figure 28: In-cylinder temperature vs. CAD histories for cases 1-5 calculated on the sector mesh

The predicted turbulent kinetic energy, TKE, and turbulent viscosity distributions are presented in Fig-

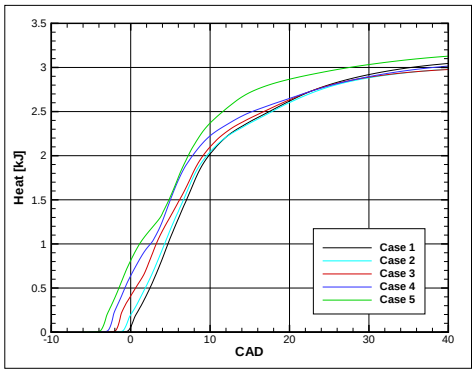

Figure 29: In-cylinder integrated heat release vs. CAD histories for cases 1-5 calculated on the sector mesh

ure 30 and 31. From TKE distributions follow that split injections create two peaks on the TKE curves, but the second maximum does not reach the value which is characteristic of a single injection. It means that for the cases with long dwell between the injections, it is difficult to expect only hydrodynamic impact on the flow-field that can increase the air entrainment and enhance soot oxidation as argued. The turbulent viscosity was also predicted lower for the cases with the long dwell times compared to the case of the single injection.

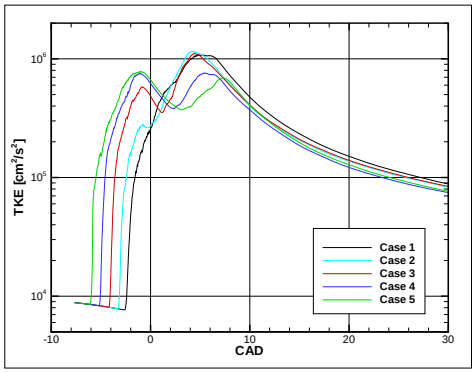

Figure 30: In-cylinder Turbulent kinetic energy vs. CAD histories for cases 1-5 calculated on the sector mesh

CONCLUSIONS

In order to investigate the effects of split injection on emission formation and engine performance, experiments was carried out using a heavy duty single cylinder Diesel engine. Split injections with varied dwell time and start of injection were investigated and compared with single injection cases. The tests were performed at low load without EGR, for four different SOI. The experimental data were compared to, and validated against numerical simulations. The major findings were:

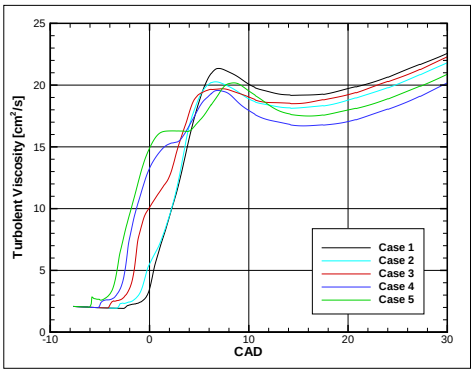

Figure 31: In-cylinder Turbulent viscosity vs. CAD histories for cases 1-5 calculated on the sector mesh

- Simultaneously reduction of NO_x and BSFC were achieved for split injections with short dwell times. In addition, no soot penalty could be detected. However, the dwell time had to be kept to a minimum resulting in a rate shaped injection rate rather than a split injection. Longer dwell times gave both increased NO_x levels and BSFC. It is therefore important to keep dwell times to a minimum when using split injections to reduce NO_x engine out emissions.

- Both CO and HC were at rather high levels. Split injections gave higher engine out emissions compared to the reference cases (single injections). Under mixing and locally fuel rich areas is believed to be the major reason for high emissions. No clear relation between dwell time and emission levels were identified.

Thus split injections with a short dwell using a common rail piezo-electric common rail injector can be used to reduce NO_x emissions and brake specific fuel consumption without increasing soot emissions at low load.

ACKNOWLEDGEMENT

The authors would like to thank the Combustion Engine Research Center at Chalmers University of Technology for the support of this project.

References

[1] Statistiska centralbyrån. http://www.scb.se/, jan 2005.

[2] T. C. Tow, D. A. Pierpoint, and R. D. Reitz. Reducing particulate and NOx emissions by using multiple injections in a heay duty D.I. diesel engine, SAE 940897. SAE, 1994.

[3] D. A. Nehmer and R. D. Reitz. Measurement of the effect of injection rate and split injections on diesel engine soot and NOx emissions, SAE 940668. In *Diesel Combustion Processes and Emision Control (SP-1028)*. SAE, feb 1994.

[4] Han Zhiyu, Uludogan All, Hampson Gregory J., and Reitz Rolf D. Mechanism of soot and NO_x emission reduction using multiple-injection in a diesel engine, SAE 960633. In *Multidimensional Engine Modelling (SP1169)*. SAE, 1996.

[5] Babu A. K. and Devaradjane G. Control of diesel engine pollutants by split injection method using multizone model, SAE 2001-28-0007. In *Second International SAE India Mobility Conference Technology Directions for Clean, Safe and Efficient Vehicles*. SAE, 2001.

[6] Yuyin Zhang and Nishida Keiya. Vapor/liquid behaviours in split-injection D.I. diesel sprays in a 2-D model combustion chamber, SAE 2003-01-1837. SAE, may 2003.

[7] Yuyin Zhang and Nishida Keiya. Effect of injection temporal splitting on the characteristics of fuel-air mixture formation in a common rail diesel spray. *Proceedings of the Institution of Mechanical Engineers, Part D: Journal of Automobile Engineering*, 218(3):323–331, may 2003.

[8] Kenji Amagai, Yukihiro Hashimoto, and Masataka Arai. Ignition and combustion characteristics of two-stage injection diesel spray. In *JSAE Review*, volume 20, pages 401–411. JSAE, jul 1999.

[9] Lionel Chrisopher Ganippa, Sven Andersson, and Jerzy Chomiak. Transient measurements of discharge coefficents of diesel nozzles, SAE 2000-01-2788. In *Combustion and emissions formation in SI and diesel engines (SP-1562)*, Journal of Engines. SAE, okt 2000.

[10] Tobias Husberg, Vittorio Manente, Rickard Ehleskog, and Sven Andersson. Fuel flow impingement measurements on multi-orifice diesel nozzles, SAE 2006-01-1552. SAE, mar 2006.

[11] Golovitchev V.I., Tanaka K. Atarashiya, K., and Yamada S. Towards universal edc-based combustion model for compression ignited engine simulations, SAE 2003-01-1849.

[12] Kong S.C., Han Z.W., and Reitz R.D. The development and application of a diesel ignition and combustion model for multidimensional engine simulations. SAE 950278. *Journal of Engines*, 104:502–518, 1995.

[13] Warnatz J., Maas U., and Dibble R.W. *Combustion – Physical and Chemical Fundamentals, Modeling and Simulation, Experiments, Pollutant Formation*. Springer-Verlag, 2nd edition, 1999.

[14] John B. Heywood. *Internal Combustion Engine Fundamentals*. McGraw-Hill book company, 1988.